Journal of New Materials for Electrochemical Systems 21, 097-102 (2018)

Nanocomposite Sheets Composed of Polyaniline Nanoparticles and Graphene Oxide as Electrode Materials for High-performance Supercapacitor

Shuhua Pang[1,§], Weiliang Chen[1,§], Zhewei Yang[1,§], Zheng Liu[1,2,§], Xin Fan[1,*] and Xu Xu[1,†]

[1]Key Laboratory of New Processing Technology for Nonferrous Metal and Materials of Ministry of Education, College of Materials Science & Engineering, Guilin University of Technology, Guilin 541004, China
[2]BengBu Center of Product Quality Supervising & Inspection, BengBu 233000, China

Received: October 12, 2017, Accepted: January 06, 2018, Available online: April 27, 2018

Abstract: *Composite materials based on the combination of graphene oxide and PANI are expected not only to improve the PANI conductivity, but also relieve graphene oxide aggregation via a synergistic effect. We report an easy synthesis of a polyaniline/graphene oxide (PGO) composite with a relatively high specific capacitance by chemical oxidation polymerization. As the employ of phytic acid and increasing aniline monomer concentration, more and more PANI nanoparticles deposited into the interval between GO layers. PGO_3 composite exhibits the largest specific capacitance (349 $F{\cdot}g^{-1}$) and PGO_4 composite follows (314 $F{\cdot}g^{-1}$), whereas PGO has a minimal specific capacitance (206 $F{\cdot}g^{-1}$). The enhanced capacitance originates from the high capacitance of more PANI nanoparticles and better configuration as well as higher surface area of PGO_3 and PGO_4 composites for fast ion transport. The as-prepared PGO_3 sheets composite with improved electrochemical performance is a promising electrode material for supercapacitor.*

Keywords: nanocomposite; polyaniline; graphene oxide sheets; electrode materials; high-performance

1. INTRODUCTION

Supercapacitor, also known as electrochemical capacitor (EC), is one of the most promising energy storage devices and has attracted enormous attention in recent years because of their unique properties including high specific power, excellent cycle stability and environmental friendliness, compared to the batteries and conventional electrolytic capacitors [1-5]. Electrode materials, namely, active materials in electrodes of supercapacitors, have significant effects on the capability, delivery rates and efficiency of energy storage devices. Of the various materials investigated as supercapacitor electrodes, conducting polymers [6-8], nanoscale carbon-based materials [3,9-12] and certain metal oxides [13-15] achieved good results due to high conductivity, large surface area and excellent pseudocapacitive properties. Due to their high specific surface area and excellent conductivity, nanostructured carbon materials are promising electrode materials for supercapacitors [10-12,16]. However, the capacitance of carbon materials is ascribed to the electrical double layer at an electrode/electrolyte interface, which is highly dependent on the specific area of the electrode [9,17]. Due to unavoidable aggregation of graphene nanosheets, nanostructured carbon materials exhibited unsatisfactory capacitance performance [18]. Compared with carbon materials, conducting polymers show much higher capacitance due to the pseudocapacitance of the redox reaction of electrode material [6,8,19,20]. However, the poor cycle life limits their real application in supercapacitors. In order to avoid the drawback of single material and to combine the excellent properties of a variety of electrode materials, nanocomposites of conducting polymers and carbon materials have been investigated to improve the electrochemical performance of electrode materials [21-28]. The special synergistic effects between various components endow electrode materials with distinguished electrochemical performance [29,30]. Liu et al. [23] employed template-free electrodeposition method to synthesize highly ordered polyaniline nanocone arrays on three-dimensional graphene network, the material remains 93.2% of initial capacitance after 1000 cycles of charging/discharging test. Graphene/polyaniline (PANI) nanocomposites prepared by Xie's group [24] showed that the incorporation of PANI nanoparticles could effectively reduce the layer-to-layer stacking of graphene

[§]These authors contributed equally to this work.
To whom correspondence should be addressed:
Email: [*]xfan@glut.edu.cn; [†]260290258@qq.com

and the nanocomposites possessed superior electrochemical performance as supercapacitors. Nanocomposites of sulfonic polyaniline nanoarrays on graphene nanosheets, [25] PANI encapsulating graphene oxide nanocomposites [26], hierarchical nanocomposites of polyaniline nanowire arrays on graphene oxide sheets[15] and carboxyl-functionalized graphene oxide-polyaniline composite [27] was synthesized for supercapacitor electrode materials and showed good synergistic effect. Heavily oxygenated graphene oxide (GO) sheets possess a number of carbonyl, hydroxyl and epoxy groups bound on the basal planes besides of partial oxygen-containing groups located at the edges [28]. Nevertheless, most of previous studies on graphene oxide-PANI composites only utilized the edged carboxyl groups to bond aniline, leaving the abundant basal oxygen-containing groups intact [31-36], which means PANI freely dangled at the edges of graphene sheets rather than at the basal planes. Liu's group [27] aligned PANI on GO sheets by oxalic acid (HOOC-COOH) to form hierarchical nano-composites, in which the various surface oxygen-containing groups at the basal planes provide active sites for PANI heterogeneous nucleation.

Herein, we try to make the best use of the basal oxygen-containing groups to achieve orderly constructed PANI/GO nanosheets by chemical oxidative polymerization. Phytic acid, as a kind of strong acid with favorable electrical conductivity, possesses 6 electronegative phosphate groups, providing 12 hydroxyl groups and more reaction sites than oxalic acid, which is more benefit for the integration of GO and phytic acid as well as preventing the aggregation of GO. Therefore, in order to avoid the aggregation of GO in the preparation process, we take advantage of hydroxyl groups of phytic acid to form hydrogen bonds with oxygen-containing groups on the surface of GO. It can not only restrain the agglomeration of GO sheets and thus facilitate the formation of a stable and orderly composite structure, but also provide a lot of active sites through hydrogen bonds derived from oxygen atom on the opposite side of hydroxyl group in phosphate group of phytic acid and -NH of aniline molecule for polymerization of aniline monomers into PANI by heterogeneous nucleation. The as-prepared GO-based nanosheet composites covered with uniform PANI nanoparticles demonstrated improved electrochemical performance as a promising electrode material for supercapacitor thanks to its stable structure and firm combination between GO and PANI.

2. EXPERIMENTAL MATERIALS

2.1. Synthesis of PANI/GO nanocomposite

Aniline and phytic acid were purchased from Aladdin and was distilled before use. Ammonium persulfate (APS)， hydrochloric acid and ethanol (Xilong Chemical Co. Ltd., Shantou, China) were in analytical grade and used as received. GO was prepared in our lab from natural graphite powder by a modified Hummers method [37].

In a typical experiment, 20 mg of graphene oxide and certain phytic acid were dispersed into 80 mL deionized water with sonication for 1 h. Then 0.5 mL of aniline was added into the mixture aqueous solution and stirred for 0.5 h in a ice bath to obtain a homogeneous solution. After this ,10 mL of APS aqueous solution (1.2498 g APS, mole ration of aniline : APS=1:1) was added drop by drop into the above homogeneous solution under vigorous stirring in a ice-water bath for 12 h. Finally, the resulting PANI/GO composite was filtered and washed with deionized water and ethanol repeatedly until the filtrate was neutral. In order to investigate the influence of aniline/phytic acid molar ratio on the morphology and electrochemical properties of PANI/GO composite, PANI/GO composites with different molar ratios (aniline/phytic acid = 4, 3, 2 and 1) were prepared and denoted as PGO_4, PGO_3, PGO_2 and PGO_1. The PANI and PANI/GO composite without phytic acid (denoted as PGO) were prepared and doped by HCl for comparison. The whole preparation procedure of the PGO nano-composite is illustrated in Scheme 1.

Scheme 1. Schematic illustration for the synthesis of polyaniline/graphene oxide nanocomposite sheets

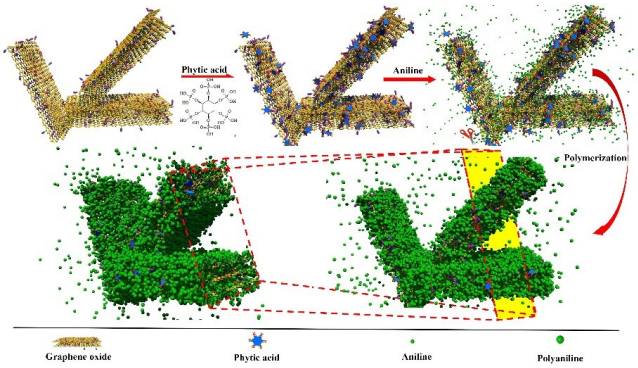

2.2. Material characterization

FTIR spectra of the GO, PANI and PGO products were recorded on a Nicolet Nexus 670 Fourier transform infrared spectrometer in the range of 4000-400 cm^{-1}. The morphologies of GO and PGO products were observed by transmission electron microscopy (TEM, JEM-2100F, Japan) and scanning electron microscopy (SEM, S4800, Japan), respectively.

2.3. Electrochemical measurements

The electrochemical measurements were performed on CHI660 electrochemical workstation in an electrolyte of 1 M H_2SO_4 solution using a three-electrode mode. The working electrode was prepared by mixing PANI/GO composite, conductive black and polytetrafluorethylene (mass ratio = 8:1:1) to yield homogeneous slurry under ultrasonic dispersion. The slurry was coated and pressed onto stainless steel mesh (the area is 1 cm^2 and the mass of active material was about 5~10 mg), then dried in a vacuum oven at 60 ^oC for 24 h. The reference electrode and counter electrode were saturated calomel electrode (SCE) and platinum electrode, respectively. Typical cyclic voltammetry (CV) performance of the PGO composites electrodes was measured between -0.2 and 0.8 V. The galvanostatic charge/discharge (GCD) tests were performed at the current densities of 0.2, 0.4, 0.6, and 0.8 $A \cdot g^{-1}$ with cutoff voltage of 0-0.8 V. Electrochemical impedance spectroscopy (EIS) tests were conducted at open circuit potential of 0.4 V in the frequency range from 100 kHz to 0.01 Hz with a sinusoidal signal of 5 mV.

All these tests were conducted at room temperature and pressure.

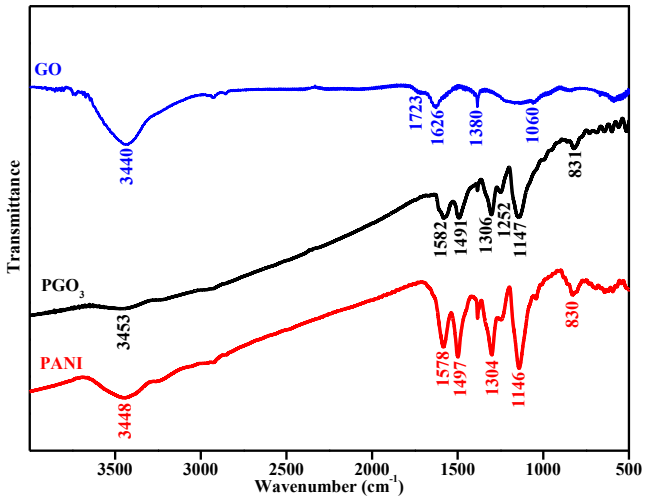

Figure 1. FTIR spectra of PANI, GO and PGO_3 samples.

The specific capacitance of the electrode was calculated by GCD curves according to equation (1):

$$Cs=(I\cdot\Delta t)/(\Delta V\cdot m) \quad (1)$$

where Cs is the specific capacitance ($F\cdot g^{-1}$), I is the current of discharge (A), Δt is the discharge time (s), m is the total mass of active material in a single electrode (g), ΔV is the potential range during discharge process (V).

3. RESULTS AND DISCUSSION

3.1. Materials structure analysis

The surfaces, defects, and edges of GO nano-sheets were decorated with various oxygen-containing functional groups such as hydroxyl, epoxy, and carboxyl groups [28,38]. These functional groups can facilitate the dispersion of GO in aqueous solution [28] and act as active sites [37] for the formation of hydrogen bonds between hydroxyl groups of phytic acid and oxygen-containing groups on the surface of GO sheets. At the same time, the negatively charged GO covered with phytic acids was expected to act as substrate to grow the nanoparticles of aniline. In the initial stage of polymerization, aniline monomers were positively charged in an acid medium and absorbed into the surface of GO sheets by electrostatic force as well as hydrogen bonds derived from isolated oxygen atom in phosphate group of phytic acid and -NH of aniline molecule, subsequently formed PANI owing to the oxidation of APS and the ordered PANI/GO configuration was formed spontaneously. The successful bonding between GO and PANI was verified by FTIR, in the meantime, the IR spectra of GO and PANI were characterized for comparison.

As shown in Fig. 1, a strong absorption at 3440 cm^{-1} is attributed to the -OH groups on the surface of GO sheets, and the absorption bands at 1723 and 1380-1060 cm^{-1} are ascribed to the C=O stretching of the -COOH and the C-O stretching of the C-OH/C-O-C groups in GO sheets, respectively [39]. All these results demonstrated the existence of plenty of oxygen-containing groups on the surface of GO sheets. What's more, a sharp band around 1626 cm^{-1} might be associated with the vibration of residual water. Compared to the PANI, the PGO_3 sample not only has similar absorption peaks but also the intensity of corresponding absorption bands remains constant, indicating that PANI was homogeneously covered on the surface of GO sheets. However, a weaker absorption band at 3448 cm^{-1} is assigned to the asymmetric stretching vibration of $-NH_2$ in PANI, which is owing to the interaction (hydrogen bonding and π-π interaction) of $-NH_2$ with phosphate groups and carboxylic acid on the surface of GO sheets.

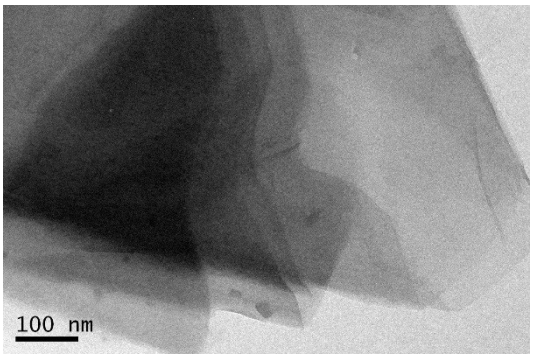

Figure 2. TEM image of graphene oxide.

TEM was used to confirm the nanosheet morphology of graphene oxide. From Fig. 2, we can clearly see that the 2D GO nanosheets composed of a few layers are loosely stacked and are almost transparent, indicating that the GO nanosheets can keep excellent dispersibility and certain interlamellar spacing via the modification of phytic acid, which is benefit for insertion of aniline monomers and subsequent tight bonding between GO and PANI after polymerization of aniline [40]. To visually learn the effect of aniline/phytic acid molar ratio on the morphology of the as-synthesized PGO composites, the surficial shape and configuration of the prepared PGO products are characterized and shown in Fig. 3 for comparison.

As is well known to all, the agglomeration is caused easily for GO in the process of preparation and application because of higher surface energy. Therefore, aniline monomers were difficult to access into the interval between GO layers and then the polymerization reactions took place on the outside surface of GO sheets (Fig. 3a and 3f). As the employ of phytic acid and increasing aniline monomer concentration, PANI nanoparticles on the outside surface of GO sheets were less and less but PANI nanoparticles in the interval between GO layers were more and more (as illustrated in scheme 1 and shown in Fig. 3b-e and 3g-j). On the one hand, PANI could form a close combination with GO sheets by way of phytic acid. On the other hand, in the polymerization process of aniline monomers on the surface of GO sheets, there were two nucleation modes: homogeneous nucleation and heterogeneous nucleation. When the aniline monomer concentration was low, aniline monomers tended to polymerize into PANI nanoparticles through heterogeneous nucleation on the edge of GO sheets. While the increase of aniline monomer concentration, aniline monomers tended to polymerize into PANI nanoparticles via homogeneous nucleation on the active sites of GO sheets. When the aniline/phytic acid molar ratio increased up to 3 or more, the surfaces of GO sheets were fully and

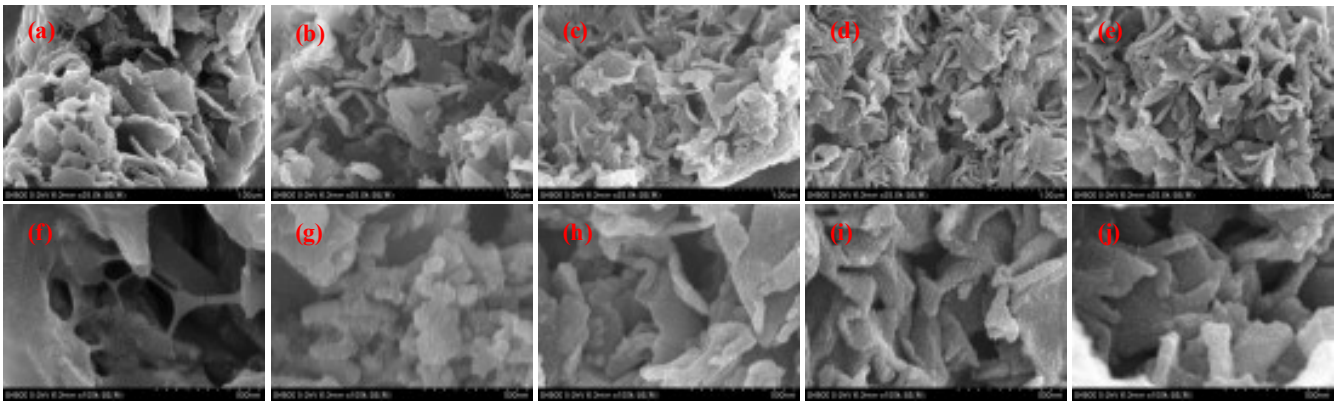

Figure 3. SEM images of PGO(a,f), PGO_1(b,g), PGO_2(c,h), PGO_3(d,i) and PGO_4(e,j) samples.

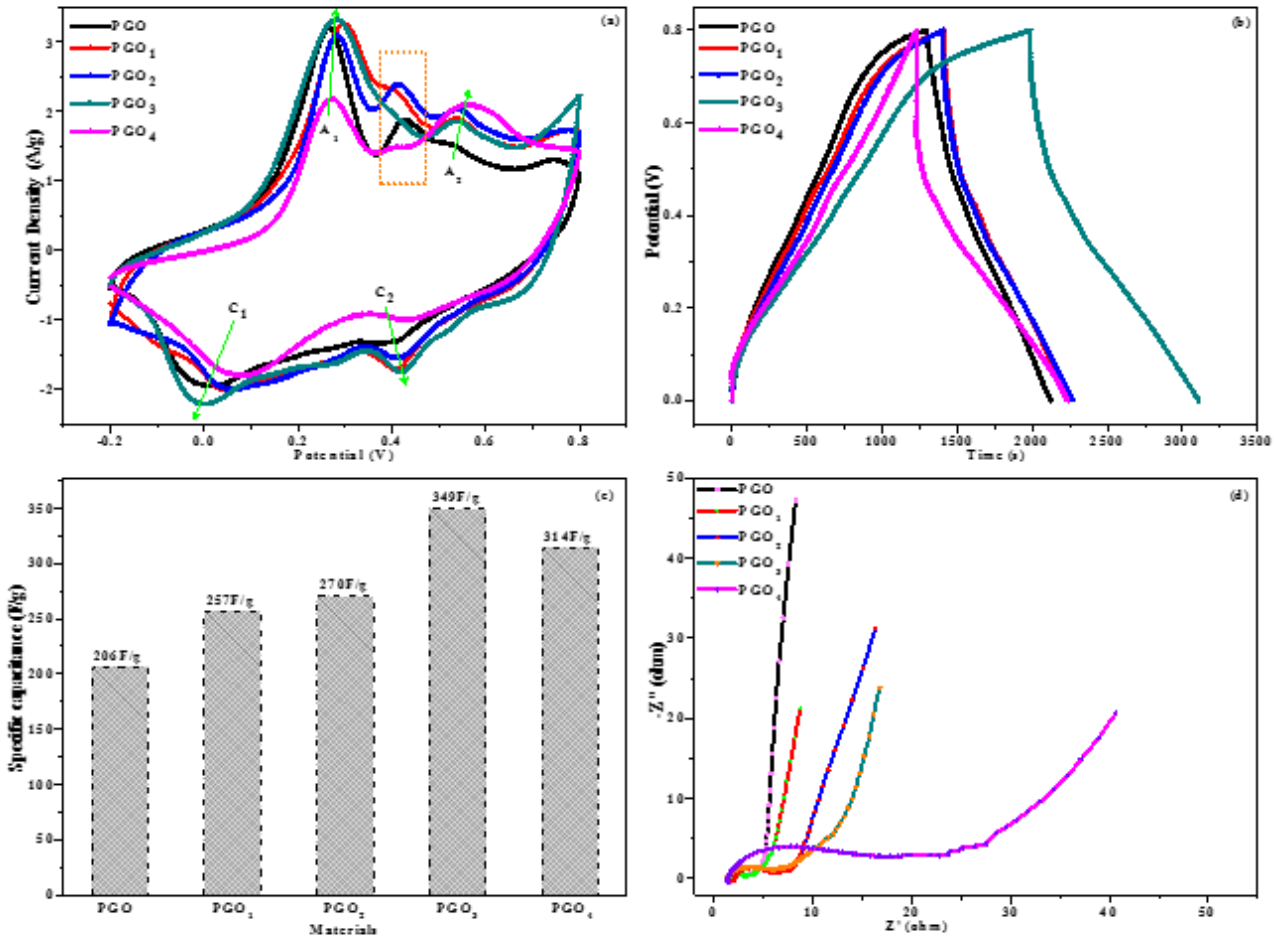

Figure 4. CV curves at scan rate of 5 $mV \cdot s^{-1}$(a), GCD curves(b) and specific capacitance at current density of 0.2 $A \cdot g^{-1}$(c), and Nyquist plots(d) for PGO samples.

uniformly covered by PANI nanoparticles, which is due to strong affinity between the GO sheets with negatively charged oxygen-containing groups and PANI nanoparticles with positively charged amine nitrogen groups.

3.2. Electrochemical properties

The electrochemical performance of PGO composites was examined by CV, GCD tests, and electrochemical impedance spectroscopy. Fig. 4a shows the CV curves of PGO composites in 1 M H_2SO_4 at scan rate of 5 $mV \cdot g^{-1}$ in the range of -0.2 to 0.8 V vs SCE. Ap-

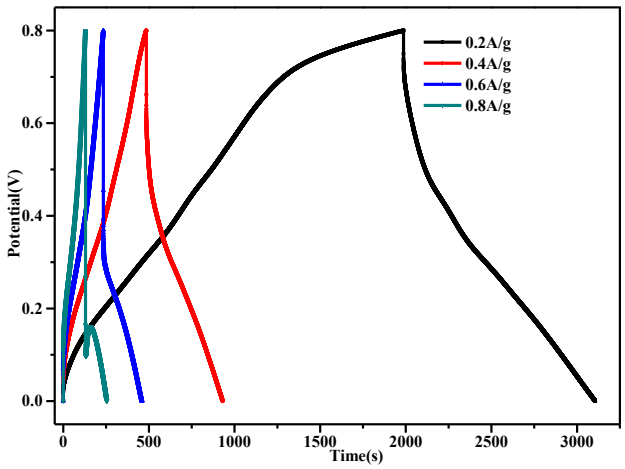

Figure 5. GCD curves of PGO_3 at different current densities.

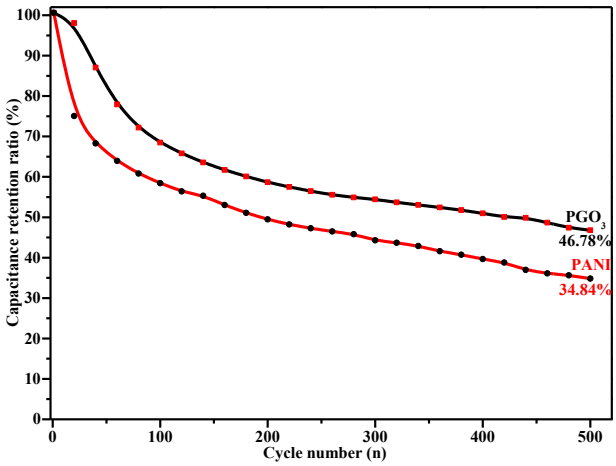

Figure 6. Capacitance retention ratios of PGO_3 and PANI samples.

parently, there are two pairs of redox peaks in all the CV curves, which correspond to the doping-dedoping transitions of different PANI forms, resulting in the pseudocapacitance for the electrode materials. A_1 and A_2 are assigned to the transitions of leucoemeraldine salt (LS) to emeraldine salt (ES) and ES to pernigraniline salt (PS), and C_1 and C_2 are their reversible transitions, respectively. Furthermore, the CV curves of PGO composites are relatively rectangular in shape, indicating excellent capacitance behavior [41,42]. Fig. 4b shows the GCD curves of PGO composites. At the same scan rate, the larger current response of the PGO composites means the higher capacitance according to the equation (1). Obviously, as shown in Fig. 4c, PGO_3 composite exhibits the largest specific capacitance (349 $F \cdot g^{-1}$) and PGO_4 composite follows (314 $F \cdot g^{-1}$), whereas PGO has a minimal specific capacitance (206 $F \cdot g^{-1}$). The enhanced capacitance originates from the high capacitance of more PANI nanoparticles [43] and better configuration as well as higher surface area of PGO_3 and PGO_4 composites for fast ion transport. Electrochemical impedance spectroscopy was carried out to further study the kinetics of the electrode process, that is, the interaction between electrode and electrolyte. EIS of PGO composites was analyzed by means of Nyquist plots, and the results are displayed in Fig. 4d. All the plots exhibited two segments, which consist of an approximate semicircle at high-frequency region and a slope line (Warburg region) at low-frequency region, indicating that the electrode process is in the control of both charge transfer and diffusion processes, respectively [32,33]. The interfacial charge transfer resistance (R_{ct}) between electrode and electrolyte is responsible for the generation of the incomplete semicircle [34,35]. From Fig. 4d, the R_{ct} values of PGO, PGO_1, PGO_2, PGO_3 and PGO_4 composites are 1.09, 1.32, 3.70, 3.38 and 13.00 Ω, respectively, indicating that PGO and PGO_1 composites show lower R_{ct} than the other PGO composites. It is due to the fact that a few PANI nanoparticles were covered on the surface of GO sheets, hence, vast GO sheets with good conductivity and fast electron transportation could efficiently reduce the inner resistance of PGO products. At lower frequency, the Nyquist plot of PGO shows steeper slope rate, thereby suggesting the shorter ion-diffusion pathways. As increasing the aniline concentration, the R_{ct} of PGO composites is gradually larger and larger, in the meantime, the slope rate is smaller and smaller, which is attributed to more and more PANI nanoparticles on the GO sheets, prolonging the ion-diffusion and electron transportation pathways compared with GO sheets.

GCD curves of PGO_3 composite were performed at different current densities (Fig. 5). The shape of all charge/discharge curves is nearly linear and symmetric, which is characteristic of a good capacitance. At 0.2 $A \cdot g^{-1}$, the specific capacitance of graphene/PANI composites is 349 $F \cdot g^{-1}$, and even at 0.8 $A \cdot g^{-1}$, the specific capacitance is 155 $F \cdot g^{-1}$. The high specific capacitance of PGO_3 composite results from the high surface area and stable well-organized space structure of the composites. The capacitances of PGO_3 composites are higher than those of previously reported graphene/PANI composites [26] and GO-PANI composite [30]. The cycling life of PGO_3 composite and PANI was tested at scan rate of 50 $mV \cdot s^{-1}$ (Fig. 6). After 500 cycles, the capacitance of PGO_3 composite and PANI remains about 46.78% and 34.84% of initial performance, respectviely, indicating improved cycling performance of PGO_3 composite owing to successful bonding interaction and synergistic effect between PANI and graphene [15].

4. CONCLUSIONS

In summary, GO-based nanosheet composites covered with uniform PANI nanoparticles were successfully synthesized by a chemical oxidative polymerization method at the presence of phytic acid. The aniline/phytic acid molar ratio plays a significant effect on the morphologies of PGO composites consequently affects the electrochemical properties strongly. As increasing the aniline concentration, more and more PANI nanoparticles deposited on the GO sheets, improving the specific capacitance of PGO composites but prolonging the ion-diffusion and electron transportation pathways compared with GO sheets. Owing to successful bonding interaction and synergistic effect between PANI and graphene, cycling performance of PGO_3 composite was too advanced. Consequently, PGO_3 nanosheet composites with a relatively high specific capacitance have a significant potential for the applications as a promising electrode material for high-performance supercapacitor.

5. ACKNOWLEDGEMENTS

This work was financially supported by Natural Science Foundation of Guangxi Province (2015GXNSFAA139277 and 2015GXNSFBA139231), Open Fund of Key Laboratory of New Processing Technology for Nonferrous Metal and Materials of Ministry of Education (14KF-1, 13KF-4), Innovation Project of Guangxi Graduate Education (YCSW2018153, JGY2018073) and National Natural Science Foundation of China (51363005).

REFERENCES

[1] G.R. Xu, J.J. Shi, W.H. Dong, Y. Wen, X.P. Min, A.P. Tang, J. Alloy. Compd., 630, 266 (2015).
[2] Q. Chen, T. Zhang, X. Qiao, D. Li, J. Yang, J. Power Sources, 234, 197 (2013).
[3] Q. Liu, Z. Tang, M. Wu, B. Liao, H. Zhou, B. Ou, G. Yu, Z. Zhou, X. Li, RSC Adv., 5, 8933 (2015).
[4] G.R. Xu, X.P. Min, Q.L. Chen, Y. Wen, A.P. Tang, H.S. Song, J. Alloy. Compd., 691, 1018 (2017).
[5] Q. Chen, Y. Wang, T. Zhang, W. Yin, J. Yang, X. Wang, Electrochimica Acta, 83, 65 (2012).
[6] Z. L. Wang, X. J. He, S. H. Ye, Y. X. Tong, G. R. Li, ACS Appl. Mater. Interfaces, 6, 642 (2014).
[7] B. Ou, W. Wang, H. Zhou, C. He. RSC Adv., 4, 52950 (2013).
[8] J. Xu, K. Wang, S. Z. Zu, B. H. Han, Z. Wei, ACS Nano, 4, 5019 (2010).
[9] D. Hulicova-Jurcakova, M. Seredych, G. Q. Lu, T. J. Bandosz, Adv. Funct. Mater., 19, 438 (2009).
[10]L. Li, E. Liu, J. Li, Y. Yang, H. Shen, Z. Huang, X. Xiang, W. Li, J. Power Sources, 195, 1516 (2010).
[11]Z. Wen, X. Wang, S. Mao, Z. Bo, H. Kim, S. Cui, G. Lu, X. Feng, J. Chen, Adv. Mater., 24, 5610 (2012).
[12]X. Li, B. Wei, Nano Energy, 2, 159 (2013).
[13]G.R. Xu, Y. Wen, X. Min, W.H. Dong, A.P. Tang, H.S. Song, Electrochim. Acta, 186, 133 (2015).
[14]D. Liu, X. Wang, X. Wang, W. Tian, J. Liu, C. Zhi, D. He, Y. Bando, D. Golberg, J. Mater. Chem. A, 1, 1952 (2013).
[15]S. P. Lim, N. M. Huang, H. M. Lim, Ceram. Int., 39, 6647 (2013).
[16]Z. S. Wu, W. C. Ren, L. B. Gao, J. P. Zhao, Z. P. Chen, B. L. Liu, D. M. Tang, B. Yu, C. B. Jiang, H. M. Cheng, ACS Nano, 3, 411 (2009).
[17]E. Frackowiak, F. Beguin, Carbon, 39, 937 (2001).
[18]Y. Wang, Z. Q. Shi, Y. Huang, Y. F. Ma, C. Y. Wang, M. M. Chen, Y. S. Chen, J. Phys. Chem. C, 113, 13103 (2009).
[19]J. Y. Huang, K. Wang, Z. X, Wei, J. Mater. Chem., 20, 1117 (2010).
[20]K. Wang, J. Y. Huan, Z. X. Wei, J. Phys. Chem. C, 114, 8062 (2010).
[21]H. Zhang, G. P. Cao, Z. Y. Wang, Y. S. Yang, Z. J. Shi, Z. N. Gu, Eletrochem. Commun., 10, 1056 (2008).
[22]H. Zhang, G. P. Cao, W. K. Wang, K. G. Yuan, B. Xu, W. F. Zhang, J. Cheng, Y. S. Yang, Electrochim. Acta, 54, 1153 (2009).
[23]M. Yu, Y. Ma, J. Liu, S. Li, Carbon, 87, 98 (2015).
[24]Z. Li, H. Zhang, Q. Liu, L. Sun, L. Stanciu, J. Xie, ACS Appl. Mater. Interfaces, 5, 2685 (2013).
[25]H. B. Zhao, J. Yang, T. T. Lin, Q. F. Lv, G. Chen, Chem. Eur. J., 21, 682 (2015).
[26]X. Li, Q. Zhong, X. Zhang, T. Li, J. Huang, Thin Solid Films, 584, 348 (2015).
[27]Y. Liu, R. Deng, Z. Wang, H. Liu, J. Mater. Chem., 22, 13619 (2012).
[28]S. Park, R. S. Ruoff, Nat. Nanotechnol., 4, 217 (2009).
[29]W. Fan, C. Zhang, W. W. Tjiu, K. P. Pramoda, C. He, T. Liu, ACS Appl. Mater. Interfaces, 5, 3382 (2013).
[30]X. Fan, Z. W. Yang, Z. Liu, Chin. J. Chem., 34, 107 (2016).
[31]H. Wang, Q. Hao, X. Yang, L. Lu, X. Wang, Electrochem. Commun., 11, 1158 (2009).
[32]K. Zhang, L. L. Zhang, X. S. Zhao, J. Wu, Chem. Mater., 22, 1392 (2010).
[33]W. L. Zhang, B. J. Park, H. J. Choi, Chem. Commun., 46, 5596 (2010).
[34]K. S. Kim, I. Y. Jeon, S. N. Ahn, Y. D. Kwon, J. B. Baek, J. Mater. Chem., 21, 7337 (2011).
[35]C. Basavaraja, W. J. Kim, Y. D. Kim, D. S. Huh, Mater. Lett., 65, 3120 (2011).
[36]L. Mao, K. Zhang, H. S. On Chan, J. Wu, J. Mater. Chem., 22, 80 (2012).
[37]D. C. Marcano, D. V. Kosynkin, J. M. Berlin, A. Sinitskii, Z. Sun, A. Slesarev, L. B. Alemany, W. Lu, J. M. Tour, ACS Nano, 4, 4806 (2010).
[38]X. G. Li, Q. F. Lv, M. R. Huang, Chem. Eur. J., 12, 1349 (2006).
[39]S. Stankovich, R. D. Piner, S. T. Nguyen, R. S. Ruoff, Carbon, 44, 3342 (2006).
[40]S. Z. Zu, B. H. Han, J. Phys. Chem. C, 113, 13651 (2009).
[41]S. Numao, K. Judai, J. Nishijo, K. Mizuuchi, N. Nishi, Carbon, 47, 306 (2009).
[42]J. Yan, T. Wei, B. Shao, F. Ma, Z. Fan, M. Zhang, C. Zheng, Y. Shang, W. Qian, F. Wei, Carbon, 48, 1731 (2010).
[43]H. Li, J. Wang, Q. Chu, Z. Wang, F. Zhang, S. Wang, J. Power Sources, 190, 578 (2009).